Intracellular Ca^{2+} Dynamics and the Stability of Ventricular Tachycardia

E. Chudin,* J. Goldhaber,# A. Garfinkel,#¶ J. Weiss,#§ and B. Kogan‖
Departments of *Biomathematics, #Medicine (Cardiology), §Physiology, ¶Physiological Science, and ‖Computer Science, University of California, Los Angeles, California 90095-1679 USA

ABSTRACT Ventricular fibrillation (VF), the major cause of sudden cardiac death, is typically preceded by ventricular tachycardia (VT), but the mechanisms underlying the transition from VT to VF are poorly understood. Intracellular Ca^{2+} overload occurs during rapid heart rates typical of VT and is also known to promote arrhythmias. We therefore studied the role of intracellular Ca^{2+} dynamics in the transition from VT to VF, using a combined experimental and mathematical modeling approach. Our results show that 1) rapid pacing of rabbit ventricular myocytes at 35°C led to increased intracellular Ca^{2+} levels and complex patterns of action potential (AP) configuration and the intracellular Ca^{2+} transients; 2) the complex patterns of the Ca^{2+} transient arose directly from the dynamics of intracellular Ca^{2+} cycling, and were not merely passive responses to beat-to-beat alterations in AP; 3) the complex Ca^{2+} dynamics were simulated in a modified version of the Luo-Rudy (LR) ventricular action potential with improved intracellular Ca^{2+} dynamics, and showed good agreement with the experimental findings in isolated myocytes; and 4) when incorporated into simulated two-dimensional cardiac tissue, this action potential model produced a form of spiral wave breakup from VT to a VF-like state in which intracellular Ca^{2+} dynamics played a key role through its influence on Ca^{2+}-sensitive membrane currents such as I_{Ca}, I_{NaCa}, and $I_{ns(Ca)}$. To the extent that spiral wave breakup is useful as a model for the transition from VT to VF, these findings suggest that intracellular Ca^{2+} dynamics may play an important role in the destabilization of VT and its degeneration into VF.

INTRODUCTION

Clinical observations (Pratt et al., 1983; Nikolic et al., 1982) indicate that ventricular fibrillation (VF) is almost always preceded by ventricular tachycardia (VT) of variable duration, ranging from a few to many beats. High-resolution cardiac mapping studies show that electrically induced VF starts as a rotating reentrant wave which is unstable and rapidly begins to meander and/or break up into multiple wavefronts, producing the electrocardiographic patterns of polymorphic VT (Gray et al., 1995) and VF (Chen et al., 1988). However, the mechanisms of the transition from VT to VF remain poorly understood. It is essential to gain a better understanding of this process to develop effective pharmacological antifibrillatory therapy.

During VT, ventricular myocytes are driven at rapid rates at which the fraction of the cardiac cycle spent in diastole decreases, leaving less time for intracellular Ca^{2+} removal and relaxation. Rapid pacing leads to elevated diastolic intracellular Ca^{2+} levels, and in many species greater filling of sarcoplasmic reticulum (SR) Ca^{2+} stores (Bassani et al., 1995; McCall et al., 1998). It is well established (Wit and Janse, 1993) that intracellular Ca^{2+} accumulation predisposes the myocardium to abnormal electrical activity such as delayed and early afterdepolarizations (DADs and EADs), and may initiate VF by itself (Koretsune and Marban, 1989; Lakatta and Guarnieri, 1993). Intracellular Ca^{2+} modulates the shape and duration of action potential (AP) through its effects on different membrane currents such as the Na^+-Ca^{2+} exchanger current (I_{NaCa}), the L-type channel current ($I_{Ca(L)}$), and the Ca^{2+}-activated nonselective current ($I_{ns(Ca)}$), thereby altering electrophysiological properties such as refractoriness and membrane depolarization rate. Thus, it is reasonable to postulate that if intracellular Ca^{2+} overload develops during VT, it could facilitate the transition into VF. To address this issue we used a combined experimental and simulation approach. First we measured intracellular Ca^{2+} transients in rabbit myocytes during pacing at rapid rates comparable to VT. Using these results, we modified the LR ventricular action potential model (Luo and Rudy, 1994; Zeng et al., 1995) to match its behavior to the experimentally obtained myocyte data. To accomplish this, we initially reformulated relaxation of intracellular Ca^{2+} transient and the mechanisms of Ca^{2+} release from the SR to incorporate recent physiological findings (Bassani et al., 1995; López-López et al., 1995; Yao et al., 1997) into the model's intracellular Ca^{2+} dynamics.

We then simulated wave propagation in a two-dimensional (2D) uniform isotropic cardiac tissue using the modified ventricular action potential model, and examined the influence of intracellular Ca^{2+} dynamics on the stability of spiral wave reentry as a model of the VT to VF transition. The results suggest that intracellular Ca^{2+} dynamics independently affect the stability of spiral wave reentry, which may contribute to the breakup of reentrant wavefronts that converts VT into VF.

Received for publication 27 April 1999 and in final form 31 August 1999.

Address reprint requests to Dr. B. Kogan, Dept. of Computer Science, UCLA, 4731E Boelter Hall, 405 Hilgard Ave., Los Angeles, CA 90095-1679. Tel.: 310-825-7393; Fax: 310-825-2273; E-mail: kogan@cs.ucla.edu.

0006-3495/99/12/2930/12 $2.00

MATERIALS AND METHODS

Cell isolation and patch clamp methods

Ventricular myocytes were isolated enzymatically from the hearts of 2–3-kg adult New Zealand white rabbits using standard methods as de-

scribed previously (Goldhaber and Liu, 1994). The cells were stored until use in standard Tyrode's solution containing (in mM): 136 NaCl, 5.4 KCl, 0.33 Na_2PO_4, 1.8 $CaCl_2$, 1 $MgCl_2$, 10 dextrose, and 10 HEPES-NaOH, pH 7.4. This storage solution was also used as the experimental bath solution. All experiments were carried out at 33–35°C.

We used the amphotericin perforated patch technique (Rae et al., 1991) to obtain whole-cell recordings of membrane voltage under current clamp conditions or to apply an action potential voltage clamp. Briefly, patch electrodes with a tip diameter of 2–3 μm and a resistance of 2–3 MΩ were dipped for ~10 s into a pipette solution containing (in mM): 140 potassium aspartate, 5 NaCl, 10 HEPES, 1 EGTA, 5 MgATP, 5 creatine phosphate, 0.05 cAMP pH 7.2 with HCl. The electrode was then back-filled using the same pipette solution containing 240 μg/ml amphotericin-B (A4888; Sigma, St. Louis, MO) added. A gigaseal was rapidly formed using standard techniques (Hammil et al., 1981). Typically, 10 min later, amphotericin pores lowered the resistance sufficiently to current or voltage clamp the cells. Membrane current and voltage were measured with an Axopatch 200 patch clamp amplifier controlled by a personal computer using a Digidata 1200 acquisition board driven by pCLAMP 6.0 software (Axon Instruments, Foster City, CA).

Fluorescence measurements

Cells were loaded with the calcium indicator fura-2 by incubating them for 20 min in bath solution containing 5 μM fura-2 AM (Molecular Probes, Eugene, OR) and 0.016% (wt/wt) pluronic (Molecular Probes). Cells were then washed twice with indicator-free bath solution and placed in a chamber mounted on the heating stage of an inverted microscope modified for simultaneous patch clamping and high-speed intracellular Ca^{2+} measurements using fura-2 (Goldhaber et al., 1991). The intensity of fura-2 fluorescence emission at 510 nm was measured by a photomultiplier during alternate excitation (1200 Hz) at 335 nm and at 405 nm. The ratio (R) of the two fluorescence wavelengths (335/405) is a reflection of intracellular Ca^{2+} (Grynkiewicz et al., 1985). Fluorescence ratios were pseudo-calibrated to intracellular [Ca^{2+}] using the following method. We assumed systolic and diastolic Ca^{2+} values of 820 and 200 nM, respectively, during pacing at 1 Hz. These values were chosen to correspond to the values used in the computer simulation. Fura-2 fluorescence ratios (R) are approximately linearly related to [Ca^{2+}] up to 10 times the K_d for Ca^{2+} binding. Thus we were able to relate the R values at systole and diastole to systolic and diastolic Ca^{2+} using the following equations:

$$\alpha = \frac{\mathrm{Ca}_{\mathrm{systole}} - \mathrm{Ca}_{\mathrm{diastole}}}{R_{\mathrm{systole}} - R_{\mathrm{diastole}}} \quad (1)$$

$$\beta = \alpha R_{\mathrm{diastole}} - \mathrm{Ca}_{\mathrm{diastole}} \quad (2)$$

$$\mathrm{Ca} = \alpha R - \beta \quad (3)$$

where $Ca_{systole}$ is the diastolic [Ca^{2+}] during pacing at 1 Hz and $Ca_{diastole}$ is the diastolic [Ca^{2+}]. $R_{systole}$ is the value of the fluorescence ratio during systole, and $R_{diastole}$ is the value of the ratio during diastole. The accuracy of this method was checked against the standard Ca^{2+} calibration equation described by Grynkiewicz et al. (1985), and gave essentially identical results.

Pacing protocols

Myocytes were either paced in the current clamp mode using a twice diastolic threshold 2 ms current pulse or in the voltage clamp mode using as the command waveform an action potential waveform recorded previously from a healthy rabbit ventricular myocyte. The action potential waveforms were recorded at several different pacing cycle lengths so that waveforms with a range of action potential durations could be used for pacing under voltage clamp conditions.

The pacing protocol was as follows: cells were paced sequentially for ~16 s at the following cycle lengths (CL) (in ms): 1000, 500, 400, 300, 180. Fura-2 fluorescence was recorded intermittently for 4-s periods to limit exposure of the cells to the ultraviolet excitation beam.

Simulation methods

Ventricular action potential generation and propagation model

AP propagation in a 2D isotropic uniform cardiac syncytium is governed by the following partial differential equation:

$$\frac{\partial V}{\partial t} = \frac{1}{C_{\mathrm{m}}}(I_{\mathrm{memb}} + I_{\mathrm{stim}}) + D\left(\frac{\partial^2 V}{\partial^2 x} + \frac{\partial^2 V}{\partial^2 y}\right) \quad (4)$$

with corresponding initial and boundary conditions, where V is the membrane potential, C_m is the membrane capacitance, I_{memb} is the total transmembrane ionic current, I_{stim} is the external transmembrane current from a stimulus, and D is the diffusion coefficient. We used the basic formulation described by Luo et al. (Luo and Rudy, 1994; Zeng et al., 1995) as our model of transmembrane currents, in which:

$$I_{\mathrm{memb}} = I_{\mathrm{Na}} + I_{\mathrm{K1}} + I_{\mathrm{Ks}} + I_{\mathrm{Kr}} + I_{\mathrm{Kp}} + I_{\mathrm{Ca(L)}} + I_{\mathrm{NaCa}} + I_{\mathrm{NaK}} + I_{\mathrm{ns(Ca)}} + I_{\mathrm{p(Ca)}} + I_{\mathrm{Nab}} + I_{\mathrm{Cab}}$$

To make Eq. 4 closed, the equations governing dynamics of intracellular Ca^{2+} and Hodgkin-Huxley-type gates are added. A complete set of equations with parameter values are given in the Appendix, and the changes we introduced to intracellular Ca^{2+} handling are described in detail below.

Reformulation of intracellular Ca^{2+} handling

Ca^{2+} extrusion from the myoplasm. Experimental evidence (Bridge et al., 1988; Barry et al., 1986) indicates that SR Ca^{2+}-ATPase and Na^+-Ca^{2+} exchanger are the dominant processes that extrude Ca^{2+} from the myoplasm. To reproduce the quantitative data obtained by Yao et al. (1997), we chose (consistent with data of Lytton et al., 1992) a Hill coefficient of 2 for the Ca^{2+}-ATPase pump and a value of 0.6 μmol/l for $K_{m,up}$. For the same reason, K_{NaCa} was increased by 10% with respect to the value used in original LR model.

Ca^{2+}-induced Ca^{2+} release by the SR. It is now widely accepted that a microscopic coupling exists between individual L-type Ca^{2+} channels and SR release channels (RyRs). RyRs (Lipp and Niggli, 1996) are likely to be grouped in functionally independent clusters or microdomains (Cannell et al., 1994). The number of recruited microdomains is believed to depend preferentially on the Ca^{2+} influx through the L-type Ca^{2+} channel, so the Ca^{2+} released from one cluster does not activate Ca^{2+} release from the other under normal physiological conditions. Based on this concept, López-López et al. (1995) proposed a formulation of Ca^{2+}-induced Ca^{2+}-release (CICR) in which probability of release is proportional to the product of probability of L-type channel opening and the probability that current through that channel will trigger Ca^{2+} release from the microdomain of RyRs. The latter was experimentally evaluated as a function of membrane potential, $P(V)$. We incorporated this formulation in the LR model by making the probability of CICR (P_{cicr}) equal to $d \cdot f \cdot f_{ca} \cdot P(V)$. Here, the product of the first three terms equals the probability of the L-type channel opening. Fig. 1 shows our approximation of the experimental data obtained for $P(V)$ by López-López et al. Our approximation provides a smooth function of $P(V)$ for all values of V with 3.5% RMS error. To reflect the fact that amount of Ca^{2+} released from the SR is regulated by SR Ca^{2+} content and to prevent unphysiological complete depletion of the SR under normal conditions (Bassani et al., 1995), we incorporated a term γ, which determines the portion of junctional SR (JSR) Ca^{2+} content available for the release (the expression for γ is given in the

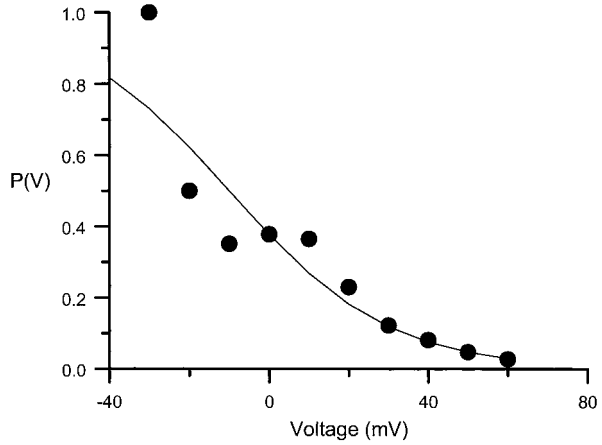

FIGURE 1 Probability $P(V)$ of a localized Ca^{2+} spark as a function of membrane potential. The black points show the data obtained experimentally by López-López et al. (1995) and the solid line shows our fit to it (see expression for $P(V)$ in Appendix).

Appendix). As a result,

$$I_{cicr} = G_{rel} \cdot P_{cicr} \cdot (\gamma[Ca^{2+}]_{jsr} - [Ca^{2+}]_i)$$

It is well known (Stern et al., 1988) that under conditions of intracellular Ca^{2+} overload spontaneous Ca^{2+} release can occur, which although initiated locally may propagate throughout the cell as a Ca^{2+} wave. The probability of spontaneous release (P_{spon}) increases with elevated myoplasmic Ca^{2+} as well as Ca^{2+} in the JSR. The spontaneous release current is given by $I_{spon} = G_{rel} \cdot P_{spon} \cdot ([Ca^{2+}]_{JSR} - [Ca^{2+}]_i)$. Here P_{spon} is similar to Hodgkin-Huxley type gate variables (see Appendix for details). Note that all JSR content is participating in spontaneous release.

T-type Ca^{2+} current. The contribution of the T-type Ca^{2+} current to both the intracellular Ca^{2+} transient and the AP has been shown to be very small (Zeng et al., 1995). Therefore, we did not include this current in our model.

Computer implementation

The model was written in C++ and ported to massively parallel supercomputers: CRAY-T3E and HP-Exemplar. Typically, on 64 processors it would require ~20 min on CRAY-T3E and 40 min on HP-EXEMPLAR to simulate 1 s of model time. Our numerical method is described in our previous study (Chudin et al., 1998). Briefly, we used an operator splitting algorithm with a time step varying between 0.005 and 0.1 ms and a fixed space step equal to 0.25 mm. Decreasing space step to 0.125 mm and minimal time step to 0.0005 ms did not significantly affect simulation results. The simulated tissue was 64×64 mm^2, larger than the critical size required to support stationary and nonstationary wave circulation. APs were initiated with -30 μA/μF of I_{st} applied for 1.3 ms in all simulations.

RESULTS

Intracellular Ca^{2+} dynamics in paced isolated ventricular myocytes: comparison with the model

Fig. 2 *A* shows APs and intracellular Ca^{2+} transients recorded at different pacing rates in an isolated rabbit ventricular myocyte, loaded with fura-2 AM, using the perforated patch clamp technique at 35°C. Note that as pacing rate increased, diastolic and systolic Ca^{2+} increased progressively. Rapid pacing eventually led to alternation of the AP and intracellular Ca^{2+} transient. To determine whether alternation was caused by the action potential or by intracellular Ca^{2+} handling, myocytes were paced in the voltage clamp mode using an action potential waveform. Under these conditions, membrane voltage was identical from beat to beat. Therefore, any beat-to-beat alterations in the intracellular Ca^{2+} transient must be an inherent property of intracellular Ca^{2+} dynamics, and not secondary to the alterations in the AP. Fig. 2 *B* shows that under these conditions, alternation of the intracellular Ca^{2+} transient still occurred at rapid pacing rates, indicating that cellular Ca^{2+} handling processes are inherently capable of nonlinear behavior. Note that at CL = 1000 ms the AP digitized for the AP clamp in Fig. 2 *B* was longer than the paced free-running AP in Fig. 2 *A* (due to the substantial cell-to-cell variation APD at long CLs in rabbit myocytes), at shorter CLs the AP clamps and paced free-running APs were comparable.

Fig. 3 *A* shows simulated AP for the modified LR model incorporating our changes in intracellular Ca^{2+} dynamics and paced at 1000 ms CL. The AP waveform and duration, as well as the maximum membrane depolarization rate, are very close to that of the original LR model. The values of diastolic and systolic $[Ca^{2+}]_i$ at this CL lie in a typical experimentally observed range (see Fig. 3 *B*). In contrast to the original LR model, however, the new model produces fractional rather than complete Ca^{2+} release from the JSR (~52% is depleted; see Fig. 4 *C*), consistent with physiological data (Bassani et al., 1995).

We next compared the values of diastolic and systolic $[Ca^{2+}]_i$ at various pacing CLs with the experimental data from isolated rabbit ventricular myocytes. The results, summarized in Fig. 3, *B* and *C*, show comparatively good agreement with experimental data. Ca^{2+} dynamics show the phenomenon of Ca^{2+} accumulation and alternans at shorter CLs. Alternans of $[Ca^{2+}]$ transient is caused by activation of the spontaneous Ca^{2+} release current, and leads to a slight (2 ms) alternans in APD. The onset of alternation in the AP and Ca^{2+} transient occurs at a bit shorter CL for the myocytes, however (see Fig. 2), and has larger amplitude.

Fig. 3 *D* demonstrates how relaxation of Ca^{2+} transient in the model (*right panel*) compares with experimental data (*left panel*) from Yao et al. (1997). We obtained close agreement for both normal relaxation and relaxation with Na^+-Ca^{2+} exchanger blocked. For normal relaxation we used CL = 4000 ms, $[Ca^{2+}]_o$ = 1.08 mmol/l, $[Na]_i$ = 10 mmol/l, $[Na]_o$ = 125 mmol/l, $[K]_i$ = 134 mmol/l, $[K]_o$ = 3.7 mmol/l. Na^+-Ca^{2+} exchanger was blocked by setting I_{NaCa} to zero. The time constants obtained for the slow (major) phase of Ca^{2+} transient relaxation with and without Na^+-Ca^{2+} exchanger block were τ_1 = 300 ms and τ_2 = 225 ms, respectively, while fits to experimental data gave τ_1 = 290 ms, τ_2 = 225 ms.

Fig. 3 *E* compares the effect of intracellular Ca^{2+} transient on the waveform of the AP. There is general agreement in details between the superimposed APs and Ca^{2+} transients in the model (*left panel*) and the myocyte (*right panel*). Both simulation and experiment show significant prolongation of APD corresponding to the larger Ca^{2+} transient. It is important to recognize the dual effect of

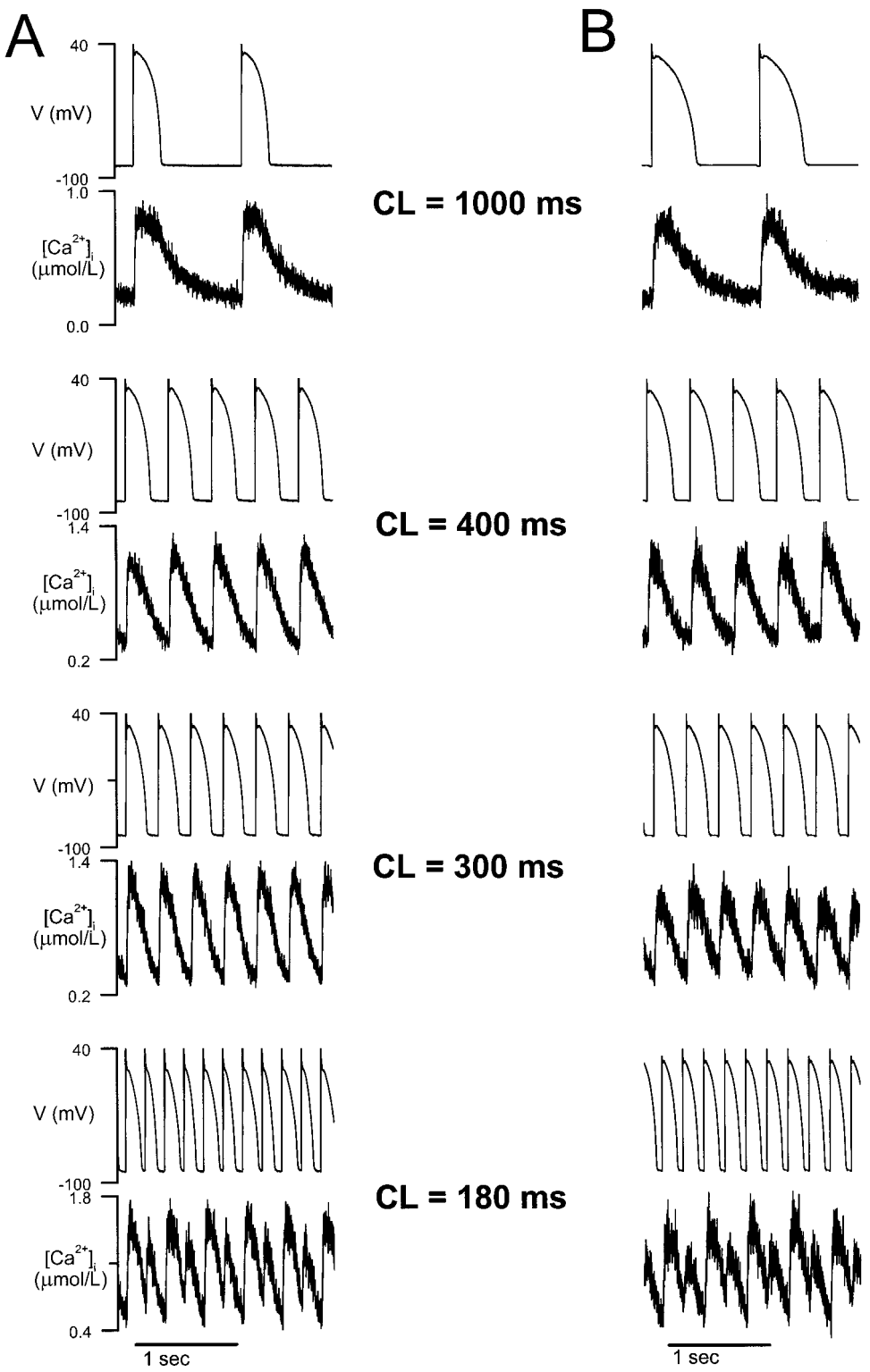

FIGURE 2 Changes in the AP and $[Ca^{2+}]_i$ transient during rapid pacing in isolated rabbit ventricular myocytes. (*A*) Membrane potential (*V*), and $[Ca^{2+}]_i$ transients during rapid pacing at cycle lengths (CL) indicated. (*B*) Same as *A*, except the myocyte is paced with an AP clamp. Note that alternation in the transient still occurs at CL = 180 ms, despite a fixed APD.

cytoplasmic free $[Ca^{2+}]$ on the APD. On one hand, a large Ca^{2+} transient tends to shorten APD by increasing $[Ca^{2+}]$-dependent inactivation of the L-type channel. On the other hand, it tends to prolong APD by enhancing inward Na^+-Ca^{2+} exchange and nonspecific Ca^{2+}-activated currents. The net result, however, in both model and experiment

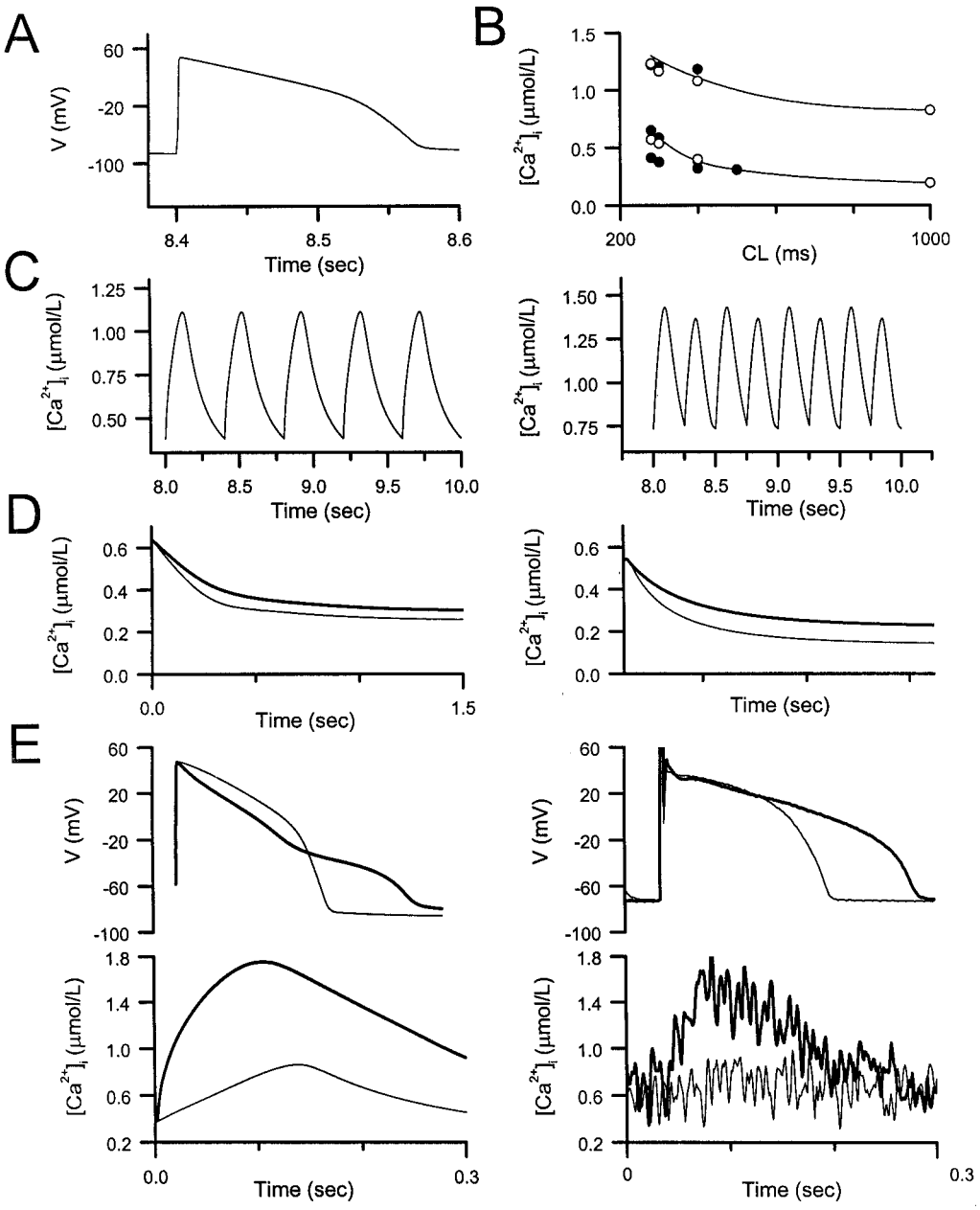

FIGURE 3 Validation of the computer model. A-AP at CL = 400 ms. B-minimum and maximum $[Ca^{2+}]_i$ during pacing with various CLs ranging from 280 ms to 1000 ms. Circles indicate experimental results (solid and unfilled symbols are from different myocytes); lines indicate computer simulation. C-$[Ca^{2+}]_i$ transients at CL = 400 ms (left panel) and CL = 250 ms (right panel). Transients display alternans at CL = 250. D-comparison of experimentally measured relaxation of $[Ca^{2+}]_i$ transients in isolated myocytes (left panel from Yao et al.) with our computer model (right panel); thin curve, control; thick lines with Na^+-Ca^+ exchange blocked. E-effect of -$[Ca^{2+}]_i$ transients on the shape of AP. The short AP (thin line) is asociated with the small -$[Ca^{2+}]_i$ transient (thin line) in both model (left) and an isolated ventricular myocyte (right) in which two successive beats during alternans were superimposed.

favored APD prolongation with the large $[Ca^{2+}]$ transients during alternans (see Fig. 3 *E*). Although I_{ks} has some dependence on $[Ca^{2+}]_i$ in the LR model, its effects on AP configuration were found to be insignificant.

Intracellular Ca^{2+} dynamics at very rapid pacing rates

During electrical induction of VF, the cycle length of the initial VT is typically in the range of 150 ms before it degenerates to VF. Neither intact ventricular tissue nor isolated ventricular myocytes can be reliably paced at such short CLs with one-to-one capture. (During the VT phase of VF, this is a reason that wavebreak occurs, causing the transition to VF.) In the model, as the CL was progressively shortened toward this range, we observed a progressive increase in the amplitude of alternans of the AP and Ca^{2+} transient (beginning at CL = 300 ms), leading to a gradual distortion of Ca^{2+} transients and AP configuration. Fig. 4 shows the time course of $[Ca^{2+}]_i$ and $[Ca^{2+}]_{JSR}$ as well as

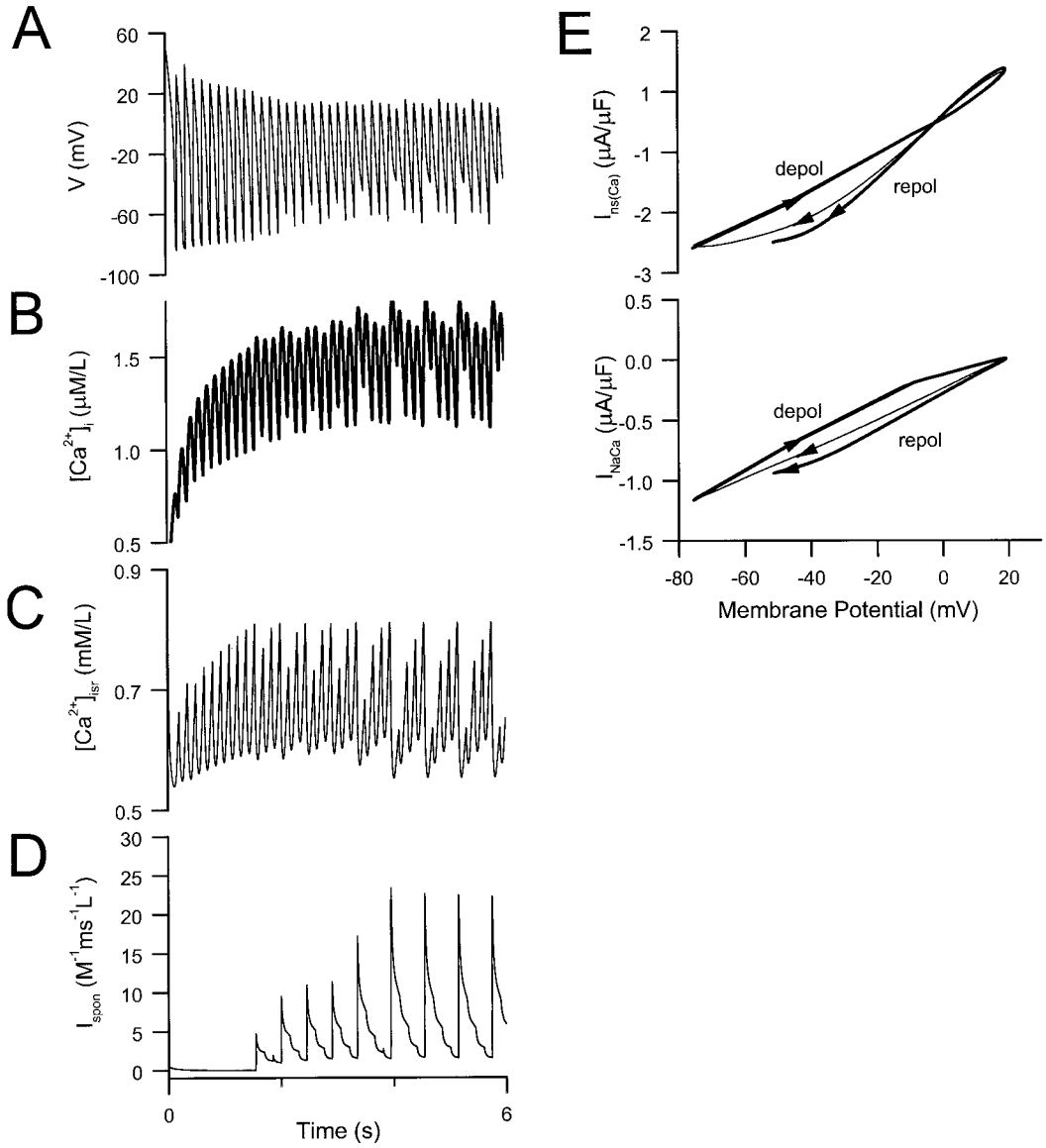

FIGURE 4 Computer model during pacing at CL = 150 ms. (*A*) AP. (*B*) Free $[Ca^{2+}]$ in myoplasm. (*C*) Free $[Ca^{2+}]$ in JSR. (*D*) Spontaneous Ca^{2+} release current. (*E*) Superimposed I_{NaCa} and $I_{ns,(Ca)}$ as functions of membrane potential during 13th an 14th APs from *A*. Currents during 14th (longer) AP are shown by bold lines.

AP and I_{spon} for a CL of 150 ms. After an initial transient period lasting ~4000 ms, stable quasiperiodic oscillations of Ca^{2+} in myoplasm and JSR were established. The quasiperiodic oscillations were caused by oscillations in spontaneous SR release, I_{spon} (see Fig. 4 *D*). The latter had a period of 600 ms (four times the period of stimulation) and began only after a significant increase in diastolic value of $[Ca^{2+}]_i$ had occurred. Diastolic values of $[Ca^{2+}]_i$ rose above 1 μmol/l. The AP was modulated by $[Ca^{2+}]_i$ oscillations through I_{NaCa}, $I_{ns(Ca)}$ (see Fig. 4 *E*), and $I_{Ca(L)}$. In Fig. 4 *E*, I_{NaCa} and $I_{ns(Ca)}$ were plotted as functions of membrane potential during both depolarization and repolarization phases of the 13th and 14th APs (from Fig. 4 *A*). The current traces diverge during the repolarization phase. Clearly, for a range of values of membrane potential, inward components of I_{NaCa}, $I_{ns(Ca)}$ are larger for larger $[Ca^{2+}]_i$ transient, thus prolonging APD. Rapid pacing also caused a significant decrease in the maximum absolute value of I_{Na} (from 360 μA/μF for CL = 1000 ms to 10 μA/μF for CL = 150 ms). Qualitatively similar oscillations in $[Ca^{2+}]_i$ with a quasiperiodic appearance were occasionally observed in rabbit ventricular myocytes during pacing. We found that the onset of quasiperiodic oscillations during rapid pacing was not very sensitive to major parameters of intracellular Ca^{2+} dynamics, although the amplitude of the oscillations was. For example, increasing K_{NaCa} and maximum rate of SR Ca^{2+} pump by 50% and G_{rel} by 30–50% did not qualitatively affect the model behavior.

Effects of intracellular Ca^{2+} dynamics on wave propagation in a 2D cardiac tissue model

We next examined the effects of intracellular Ca^{2+} dynamics on spiral wave reentry in simulated 2D cardiac tissue. We chose the diffusion coefficient D to give a conduction velocity of ~55 cm/s for a solitary plane wave. To obtain a reentrant spiral wave, the rectangular region behind the tail of the rectilinear wave was excited. Because the excitation could not spread into an unrecovered region, a point (q) appeared where the front was adjacent to the tail. This led to the curving of the wavefront around this point (see Fig. 5 *A*), which formed the tip of a spiral wave (Fig. 5, *B* and *C*). The spiral wave made four rotations with a period of 170 ms and diastolic interval of 20 ms, and then became nonstationary, with the wavefront progressively deteriorating for ~3000 ms (Fig. 5 *D*). The breakup of the spiral wave was sensitive to the "gain" in the $[Ca^{2+}]_i$ sensitivity of various Ca^{2+}-sensitive ionic currents. For example, increasing the $[Ca^{2+}]_i$ sensitivity of $I_{ns(Ca)}$ by decreasing $K_{m,ns(Ca)}$ from 1.2 μmol/l to 1.0 μmol/l facilitated breakup of the wavefront into the

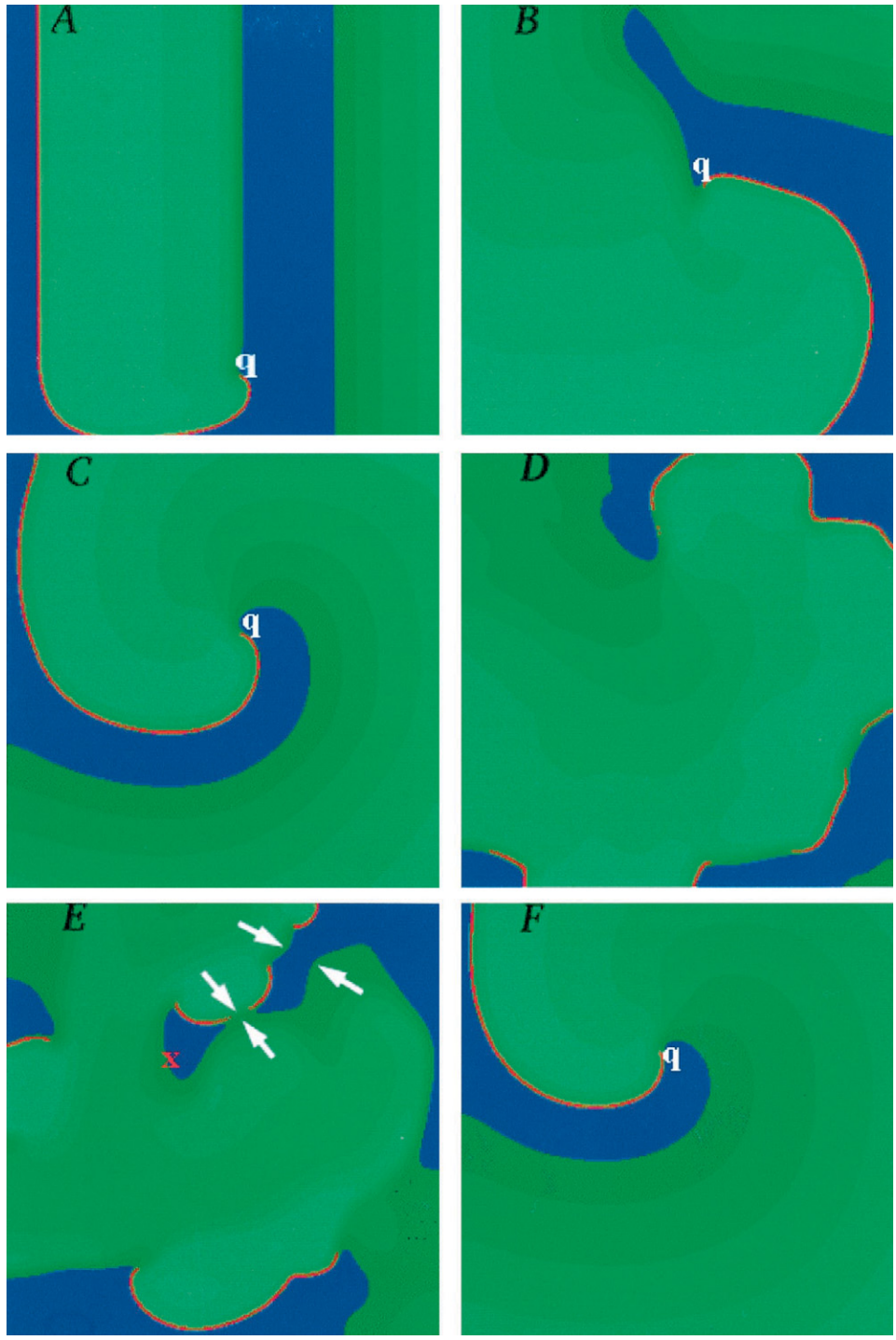

FIGURE 5 Ca^{2+} dynamics cause spiral wave breakup in simulated 2D cardiac tissue model. (*A–E*) Initiation of a spiral wave following a premature stimulus (*A* and *B*). After the spiral wave becomes established (*C*, t = 1275 ms), deformations develop (*D*, t = 4010) leading to spiral wave breakup (*E*). After spontaneous Ca^{2+} release was blocked, the multiple reentrant waves coalesced back into a single spiral. *Blue* indicates $V < -60$ mV; *green*, $V \geq -60$ mV; *red*, absolute value of $I_{memb} > 10$ μA/μF.

fibrillation-like state (Fig. 5 *E*). During spiral wave rotation, each cell in a tissue model is being rapidly excited (CL = 170 ms), which we showed in single cell simulations was sufficient to cause the conditions of intracellular Ca^{2+} overload and spontaneous Ca^{2+} release.

Analysis of APs and Ca^{2+} transients recorded from a local site in the tissue showed that the transition from the stationary to nonstationary regime started abruptly with an unusually large Ca^{2+} transient (see Fig. 6 *A*) due to spontaneous Ca^{2+} release. This caused substantial prolongation of the AP (Fig. 6 *A, top graph*), due to the increase in inward components of I_{NaCa} and $I_{ns,Ca}$, which led to marked shortening of the subsequent diastolic interval. The short diastolic interval dramatically decreased the depolarization rate of the subsequent AP (by ~5-fold) due to the incomplete recovery of I_{Na} from inactivation, which slowed the conduction velocity of the wavefront. The short diastolic interval also shortened the duration of the subsequent AP due to its restitution properties, markedly altering the wavelength (the product of APD and conduction velocity) in this region. Conversely, the short diastolic interval and altered AP affected the intracellular Ca^{2+} transient of the next beat, which further modified the AP via its feedback on Ca^{2+}-sensitive currents.

If the interaction between $[Ca^{2+}]_i$ and the Ca^{2+}-sensitive currents affecting the AP and conduction velocity is sufficiently strong, variations of restitution properties along the arm of the spiral wave grow to the point where the excitation wave can no longer propagate. Note particularly in Fig. 5 *E* that the wavebreaks occur at wavefront/waveback interactions (see *arrows*). This causes the spiral wave to break up, leading to the fibrillation-like state. In this scenario, spontaneous Ca^{2+} release acts as a gain-enhancing mechanism between $[Ca^{2+}]_i$ and Ca^{2+}-sensitive currents. As we mentioned above, if this gain was decreased by reducing the Ca^{2+} sensitivity of Ca^{2+}-sensitive currents (reducing the amplitudes of APD oscillations), then spiral wave breakup was prevented. Likewise, if the gain was decreased by eliminating spontaneous Ca^{2+} release, spiral wave breakup also did not occur. In fact, if spiral wave breakup was allowed to develop with spontaneous Ca^{2+} release mechanism intact, its subsequent elimination caused the multiple reentrant wavefronts to coalesce back into a single stationary spiral wave (Figs. 5 *F* and 6 *B*). In this case, the tip of the reformed spiral wave was shifted with respect to its original position (before start of nonstationary reentry), due to the redistribution of recovery processes during the nonstationary regime.

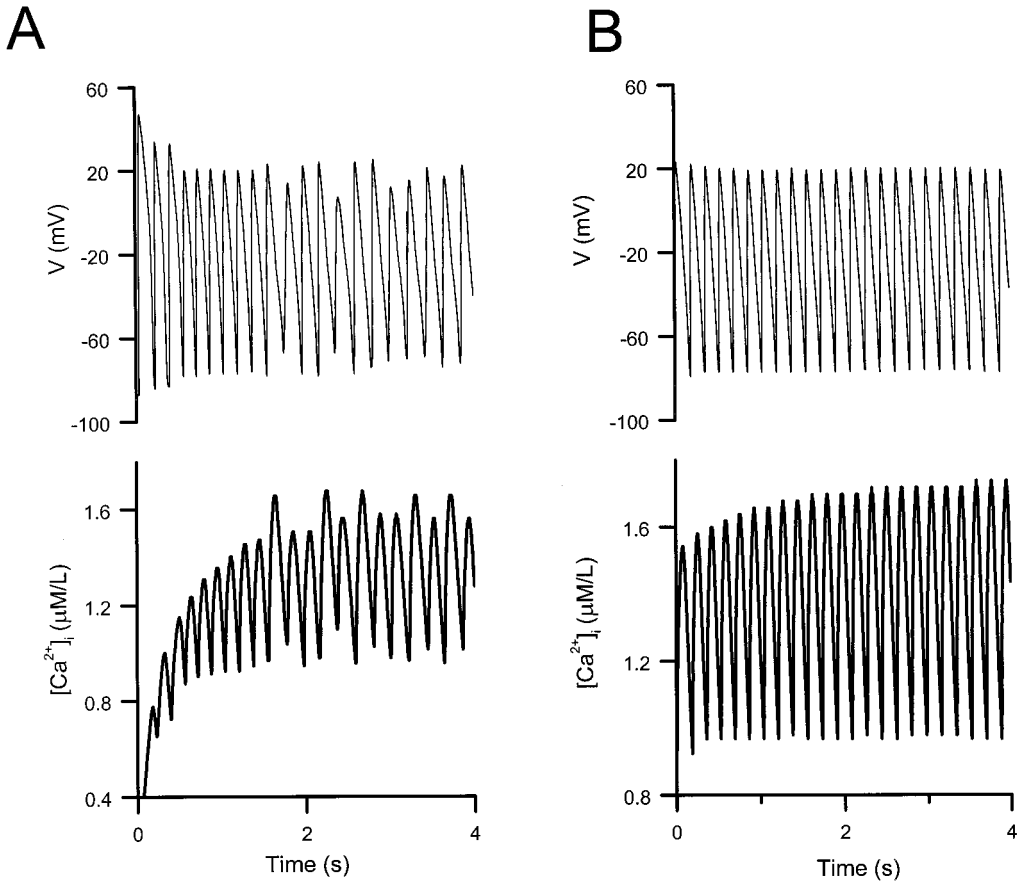

FIGURE 6 Traces of membrane potential *V* (*top*), and $[Ca^{2+}]_i$ (*bottom*) measured at a site ($Nx = 100$, $Ny = 100$; origin is at top left corner) in a simulated 2D tissue. Quasiperiodic oscillations disappeared when I_{spon} was blocked, as in Fig. 5 *F*. (*A*) *V* and $[Ca^{2+}]_i$ during development of spiral wave breakup. (*B*) *V* and $[Ca^{2+}]_i$ after the block of spontaneous Ca^{2+} release.

DISCUSSION

Intracellular Ca^{2+} overload and VF are interrelated phenomena. Indeed, increased $[Ca^{2+}]_i$ appears to play an important role in initiating VF (Wit and Janse, 1993; Lakatta and Guarnieri, 1993), and VF by itself may lead to Ca^{2+} overload conditions (Koretsune and Marban, 1989), which further maintains VF. Therefore, it is important to understand the role of Ca^{2+} dynamics in the transition from VT to VF. We investigated this issue using a combined experimental and mathematical modeling approach. Our results show that 1) rapid pacing of rabbit ventricular myocytes leads to increased intracellular Ca^{2+} levels and complex patterns of variability in the AP and the intracellular Ca^{2+} transient (Fig. 2 *A*); 2) the complex patterns of the intracellular Ca^{2+} transient arise directly from the dynamics of intracellular Ca^{2+} regulation, and are not merely passive responses to beat-to-beat alterations in AP (Fig. 2 *B*); 3) these complex Ca^{2+} dynamics have been simulated in a version of the LR ventricular action potential with modified intracellular Ca^{2+} dynamics, and show agreement with the experimental findings in isolated myocytes; and 4) when incorporated into simulated 2D cardiac tissue, this action potential model produces a form of spiral wave breakup in which intracellular Ca^{2+} dynamics play a key role through their influence on Ca^{2+}-sensitive membrane currents such as $I_{Ca(L)}$, I_{NaCa}, and $I_{ns(Ca)}$. To the extent that spiral wave breakup is useful as a model for the transition from VT to VF, these findings suggest that intracellular Ca^{2+} dynamics can play an important role in the destabilization of VT and its degeneration into VF.

Effects of rapid pacing on intracellular Ca^{2+}

The effects of pacing on intracellular Ca^{2+} in cardiac muscle have been studied before, both by direct measurements of intracellular Ca^{2+} with fluorescent dyes and by using tension as a surrogate. Alternation of the AP and Ca^{2+} transient during pacing have been analyzed in numerous studies. In most, pharmacological interventions were applied to determine whether the alternation arose primarily from electrical or mechanical processes. For example, Saitoh et al. (1989) provided pharmacologically based evidence that Ca^{2+} dynamics are the main cause of electrical and mechanical alternans in ventricular muscle, whereas recovery properties of membrane currents are the main determinants in His-Purkinje tissue. However, pharmacologic tools are never completely specific, and the range of heart rates studied in these preparations were generally slower than the typical rate of VT before it degenerates to VF. In this study, the ability to rapidly pace using action potential clamps provides a major advantage. By preventing changes in the AP from secondarily influencing intracellular Ca^{2+} dynamics, it allows direct assessment of the stability of intracellular Ca^{2+} dynamics without having to resort to pharmacological interventions. In addition, the use of the perforated patch technique ensures minimal disturbance of the cytoplasm and preservation of intact intracellular signaling pathways. Finally, we investigated a range of pacing rates directly relevant to VT and VF.

The observation that stable alternation of the Ca^{2+} transient occurred during rapid pacing with the AP clamp (in which waveform of AP is fixed) indicates that the restitution of the Ca^{2+} transient is independently influenced by other factors besides the diastolic interval. This explains the quasiperiodic behavior of the AP and Ca^{2+} transients during regular pacing (Fig. 4, *left column*): AP restitution properties contribute the oscillations of APD, which are modulated by a oscillations arising independently from the restitution properties of the intracellular Ca^{2+} transient. Perhaps it is not surprising that the interaction between these processes, when distributed spatially over a 2D tissue, can amplify the electrophysiological heterogeneities that lead to spiral wave breakup (Fig. 5).

Validity of the action potential model

The relevance of our analysis of the role of intracellular Ca^{2+} dynamics in the transition from VT to VF depends on the validity of the action potential model and its ability to accurately simulate the behavior of cardiac muscle at very rapid pacing rates. The LR model is becoming the most widely used model of ventricular AP, and therefore we chose to use it after reformulating the intracellular Ca^{2+} dynamics. Mainly, we replaced the discontinuous formulation of Ca^{2+} release from the SR in the original model by a continuous one. The advantages of this modification are that it reflects more closely the physiological mechanisms of Ca^{2+} release, and also eliminates mathematical artifacts associated with threshold and time delay properties of the model (Luo and Rudy, 1994). Our formulation provides graded depletion of the SR Ca^{2+} content (see Fig. 4 *C*), while most other models deplete the SR almost completely with each excitation, contrary to experimental data (Bassani et al., 1995).

The model parameters were adjusted to reproduce as closely as possible the experimental behavior of the isolated rabbit ventricular myocytes during rapid pacing, particularly the accumulation of intracellular Ca^{2+} and the development of alternans. In the model, the rise in the diastolic values of $[Ca^{2+}]_i$ with rapid pacing is attributed to the fact that Ca^{2+} is entering the cell through the L-type channel more rapidly than it is extruded. The increased $[Ca^{2+}]_i$ accelerates $I_{Ca,(L)}$ inactivation and enhances the I_{NaCa} and $I_{ns(Ca)}$, consequently affecting the shape of the AP. At a rate comparable to the rate of VT (150 ms), $[Ca^{2+}]_i$ reached a level sufficient to induce spontaneous SR Ca^{2+} release. The latter occurred periodically but with a period different from the CL. The interaction of two periodic processes resulted in a quasiperiodic regime. Thus, spontaneous SR Ca^{2+} release is a candidate for the postulated additional factor suggested by the experimental results which, independent of the diastolic interval, controls Ca^{2+} transient restitution. Further

studies are necessary to test this possibility. It is worthwhile to note that the original LR model produces chaotic, rather than quasiperiodic, oscillations with much larger amplitudes under the same pacing conditions (Chudin et al., 1998). This difference is caused by the discontinuous threshold nature of CICR formulation in the original LR model, which is avoided in our reformulation.

Role of intracellular Ca^{2+} dynamics in spiral wave breakup

When the modified LR model was used to simulate 2D cardiac tissue, we found that Ca^{2+} dynamics were directly responsible for causing the transition from stationary to violently meandering spiral wave reentry promoting wavebreak and a fibrillation-like state. This occurred because the complex temporal intracellular Ca^{2+} dynamics resulted in spatial inhomogeneities in intracellular $[Ca^{2+}]_i$, which amplified the inward component of the Na^+-Ca^{2+} exchanger current and the nonspecific Ca^{2+}-activated current to produce in turn electrophysiological inhomogeneities by prolonging APD. These spatial regions of prolonged repolarization interact with the wavefront during the next rotation of the spiral wave, sharply decreasing conduction velocity and causing wavebreak. This is illustrated in Fig. 5, in which the red color represents the points on the wave front where absolute value of I_{memb} current (see Eq. 4) is greater than 10 $\mu A/\mu F$ (the approximate threshold corresponding to significant participation of I_{Na} in wavefront propagation). Breaks in the red line indicate slow propagation supported by the L-type Ca^{2+} current (where I_{Na} is highly inactivated) or conduction failure. We verified that the qualitative nature of our results remained robust with respect to various aspects of CICR current such as expressions for $P(v)$, γ, and value of G_{rel}. Moreover, despite the different formulation of intracellular Ca^{2+} dynamics and different morphology of Ca^{2+} transient, the original LR model gave qualitatively similar results; that is, when its Ca^{2+} dynamics were operational, spiral wave breakup occurred due to the Ca^{2+} instability (Chudin et al., 1998).

These findings are generally consistent with studies implicating cardiac restitution properties as key determinants of spiral wave instability and breakup (Koller et al., 1998; Karma, 1994; Weiss et al., 1999). We suggest that the effects of intracellular Ca^{2+} may operate dynamically by promoting functional electrophysiological heterogeneities. By modulating various Ca^{2+}-sensitive currents, intracellular Ca^{2+} levels locally alter cardiac restitution properties. If the "gain" between intracellular Ca^{2+} and Ca^{2+}-sensitive currents affecting restitution is sufficiently high, intracellular Ca^{2+} dynamics may promote instability.

It is interesting to compare the results of our study with findings of Merillat et al., (1990), who demonstrated that Na-K pump inhibition (which leads to Ca^{2+} overload) produced VF even when spontaneous Ca^{2+} oscillations were blocked. In our study we demonstrate that such spontaneous Ca^{2+} oscillations may cause transition from VT to VF, but this does not imply that they are the only mechanism (e.g., see Weiss et al., 1999).

Limitations and implications of the study

A number of limitations should be noted in considering the implications of this study for clinical VF. We have only simulated homogeneous isotropic 2D cardiac tissue, whereas real hearts are 3D, anisotropic, and inhomogeneous. Nevertheless, if intracellular Ca^{2+} dynamics promote spiral wave instability in such a simple model, they are likely to contribute to instability in more complex models as well.

Our reformulation of intracellular Ca^{2+} dynamics improves but still grossly simplifies the real physiological situation, about which many controversies are still unsettled. The AP model contains the major, but not all of the known, Ca^{2+}-sensitive currents in heart such as Ca^{2+}-sensitive Cl^- current (Zygmunt and Gibbons, 1991) and Ca^{2+} sensitivity of I_{K1} (Zaza et al., 1998). Finally, it cannot be directly ascertained whether spontaneous Ca^{2+} release from the SR actually causes Ca^{2+} alternans in cardiac myocytes during rapid pacing, but our model reproduces Ca^{2+} alternans phenomenologically. It may be possible to gain further insight into these mechanisms by altering elements of intracellular Ca^{2+} regulation with various drugs and hormones, and studying the interplay among intracellular Ca^{2+} dynamics, the AP, and wave propagation using a combined experimental and simulation approach.

Also, our model, like most others, assumes constant $[Na^+]$ and $[K^+]$ in myoplasm. Unfortunately, our experience shows that allowing changes of these ionic concentrations causes slowly developing instabilities due to the loss of ionic balance. Undoubtedly, incorporation of $[Na^+]$ and $[K^+]$ dynamics into the cell model can illuminate other interesting phenomena. Finally, the myocyte experiments were performed at slightly lower temperature (33–35°C) than physiological, because myocytes did not tolerate sustained rapid pacing at 37°C.

Despite these limitations, our results suggest that intracellular Ca^{2+} dynamics must be considered as a potentially important factor promoting the transition of VT to VF. Altered intracellular Ca^{2+} dynamics by factors promoting intracellular Ca^{2+} overload (e.g., digitalis toxicity) or by autonomic factors (e.g., enhanced sympathetic tone) could play a role clinically in the predisposition to VT/VF and sudden cardiac death.

APPENDIX: EQUATIONS FOR IONIC CURRENTS

Cell geometry and ionic concentrations

Volumes of intracellular compartments (V_{myo}, V_{nsr}, V_{JSR}), capacitive membrane area A_{cap}, and standard ionic concentrations and all processes not mentioned below are the same as in the original publications (Luo and Rudy (1994).

Na^+-Ca^{2+} exchanger: I_{NaCa}

The same as in Luo and Rudy (1994), with the value of K_{NaCa} decreased from 2000 μA/μF to 1177 μA/μF.

Nonspecific Ca^{2+} activated current: $I_{ns(Ca)}$

The same as in Luo and Rudy (1994), with the value of $K_{m,ns(Ca)}$ decreased from 1.2 μmol/l to 1.0 μmol/l in some 2D simulations.

Ca^{2+} uptake and leakage of NSR: I_{up} and I_{leak}

$$I_{up} = v_{max} \cdot [Ca^{2+}]_i^2/(K_{m,up}^2 + [Ca^{2+}]_i^2)$$

$$v_{max} = 1.792 \cdot 10^{-3} \text{ mmol/l/ms}, \quad K_{m,up} = 0.6 \ \mu\text{mol/l}.$$

$$I_{leak} = g_{leak} \cdot ([Ca^{2+}]_{NSR} - [Ca^{2+}]_i)$$

$$g_{leak} = 1.195 \cdot 10^{-4} \text{ ms}^{-1}.$$

Translocation of Ca^{2+} from NSR to JSR: I_{tr}

The same as in Luo and Rudy (1994), with the value of τ_{tr} decreased from 180 ms to 50 ms.

CICR of JSR: I_{cicr}

$$I_{cicr} = G_{rel} \cdot d \cdot f \cdot fca \cdot P(V) \cdot (\gamma \cdot [Ca^{2+}]_{JSR} - [Ca^{2+}]_i)$$

where d is the activation gate of the L-type channel and f and fca are voltage- and calcium-dependent inactivation gates of this channel, respectively.

$$P(V) = \{1 + 1.65 \cdot \exp(V/20)\}^{-1}$$

$$\gamma = \{1 + (K_{rel}/[Ca^{2+}]_{JSR})^3\}^{-1}, \quad K_{rel} = 2.0 \text{ mmol/l}$$

$$G_{rel} = 60 \text{ ms}^{-1}$$

Spontaneous Ca^{2+} release from JSR: I_{spon}

$$I_{spon} = G_{rel} \cdot P_{spon} \cdot ([Ca^{2+}]_{JSR} - [Ca^{2+}]_i)$$

$$\frac{dP_{spon}}{dt} = \frac{P_\infty - P_{spon}}{\tau_P}$$

Here P_∞ is a continuous function of $[Ca^{2+}]_{JSR}$ and $[Ca^{2+}]_i$:

$$P_\infty = 0 \quad \text{if} \quad [Ca^{2+}]_{JSR} < K3 \quad \text{or} \quad [Ca^{2+}]_i < K4$$

$$P_\infty = 1 \quad \text{if} \quad [Ca^{2+}]_{JSR} > K1 \quad \text{and} \quad [Ca^{2+}]_i > K2.$$

$$P_\infty = \frac{([Ca^{2+}]_{JSR} - K3) \cdot ([Ca^{2+}]_i - K4)}{\{(K1 - K3) \cdot (K2 - K4)\}},$$

$$\text{if} \quad K3 < [Ca^{2+}]_{JSR} < K1 \quad \text{and} \quad K4 < [Ca^{2+}]_i < K2.$$

$$P_\infty = ([Ca^{2+}]_{JSR} - K3)/(K1 - K3),$$

$$\text{if} \quad K3 < [Ca^{2+}]_{JSR} < K1 \quad \text{and} \quad [Ca^{2+}]_i > K2$$

$$P_\infty = ([Ca^{2+}]_i - K4)/(K2 - K4),$$

$$\text{if} \quad K4 < [Ca^{2+}]_i < K2 \quad \text{and} \quad [Ca^{2+}]_{JSR} > K1$$

$$\tau_P = 20 + (1 - P_\infty) \cdot 200 \text{ ms}.$$

where K1 = 1.4 mmol/l, K2 = 1.3 μmol/l, K3 = 0.8 mmol/l, K4 = 0.7 μmol/l.

Dynamic changes of Ca^{2+} in myoplasm and SR

$$\frac{d[Ca^{2+}]_{myo}}{dt} = -(I_{Ca,L} + I_{Ca,b} + I_{p(Ca)} - 2I_{NaCa}) \frac{A_{cap}}{(2V_{myo}F)} - (I_{up} - I_{leak}) \frac{V_{nsr}}{V_{myo}} + (I_{cicr} + I_{spon}) \frac{V_{jsr}}{V_{myo}}$$

$$\frac{d[Ca^{2+}]_{JSR,total}}{dt} = I_{tr} - (I_{cicr} + I_{spon})$$

$$\frac{d[Ca^{2+}]_{NSR}}{dt} = (I_{up} - I_{leak}) - I_{tr} \frac{V_{jsr}}{V_{nsr}}$$

Here F is Faraday constant. Note that $[Ca^{2+}]_{myo}$ and $[Ca^{2+}]_{JSR,total}$ are total Ca^{2+} concentrations in myoplasm and JSR, respectively.

This study was supported by National Institutes of Health Grant SCOR in Sudden Cardiac Death P50 HL52319, National Institutes of Health Training Grant GM08185, the Laubisch Fund and the Kawata Endowment. The supercomputers used for this investigation were provided by funding from NASA Offices Mission to Planet Earth, Aeronautics, and Space Sciences and National Energy Research Scientific Computing Center, which is supported by the Office of Energy Research of the U.S. Department of Energy under Contract No. DE-AC03-76SF00098.

REFERENCES

Barry, W. H., C. A. Rasmussen, Jr., H. Ishida, and J. H. Bridge. 1986. External Na-independent Ca extrusion in cultured ventricular cells. Magnitude and functional significance. *J. Gen. Physiol.* 88:393–411.

Bassani, J. W., W. Yuan, and D. M. Bers. 1995. Fractional SR Ca release is regulated by trigger Ca and SR Ca content in cardiac myocytes. *Am. J. Physiol.* 268:C1313–C1319.

Bridge, J. H., K. W. Spitzer, and P. R. Ershler. 1988. Relaxation of isolated ventricular cardiomyocytes by a voltage-dependent process [published erratum appears in Science 1988 Dec 9;242(4884):1361]. *Science.* 241: 823–825.

Cannell, M. B., H. Cheng, and W. J. Lederer. 1994. Spatial non-uniformities in $[Ca^{2+}]_i$ during excitation-contraction coupling in cardiac myocytes. *Biophys. J.* 67:1942–1956.

Chen, P. S., P. D. Wolf, E. G. Dixon, N. D. Danieley, D. W. Frazier, W. M. Smith, and R. E. Ideker. 1988. Mechanism of ventricular vulnerability to single premature stimuli in open-chest dogs. *Circ. Res.* 62:1191–2209.

Chudin, E., A. Garfinkel, J. Weiss, W. Karplus, and B. Kogan. 1998. Wave propagation in cardiac tissue and effects of intracellular calcium dynamics (computer simulation study). *Prog. Biophys. Mol. Biol.* 69:225–236.

Goldhaber, J. I., and E. Liu. 1994. Excitation-contraction coupling in single guinea-pig ventricular myocytes exposed to hydrogen peroxide. *J. Physiol.* 477:135–147.

Goldhaber, J. I., J. M. Parker, and J. N. Weiss. 1991. Mechanisms of excitation-contraction coupling failure during metabolic inhibition in guinea-pig ventricular myocytes. *J. Physiol.* 443:371–386.

Gray, R. A., J. Jalife, A. Panfilov, W. T. Baxter, C. Cabo, J. M. Davidenko, and A. M. Pertsov. 1995. Nonstationary vortexlike reentrant activity as a mechanism of polymorphic ventricular tachycardia in the isolated rabbit heart. *Circulation.* 91:2454–2469.

Grynkiewicz, G., M. Poenie, and R. Y. Tsien. 1985. A new generation of Ca2+ indicators with greatly improved fluorescence properties. *J. Biol. Chem.* 260:3440–3450.

Hammil, O. P., A. Marty, E. Neher, E. Sakmann, and F. J. Sigworth. 1981. Improved patch clamp techniques for high resolution current recording from cells and cell-free membrane patches. *Pfluger's Arch.* 391:85–100.

Karma, A. 1994. Electrical alternans and spiral wave breakup in cardiac tissue. *Chaos.* 4:461–72.

Koller, M. L., M. L. Riccio, and R. F. Gilmour. 1998. Dynamic restitution of the action potential during electrical alternans and ventricular fibrillation. *Am. J. Physiol.* 275:H1635–H1642.

Koretsune, Y., and E. Marban. 1989. Cell calcium in the pathophysiology of ventricular fibrillation and in the pathogenesis of postarrhythmic contractile dysfunction. *Circulation.* 80:369–379.

Lakatta, E. G., and T. Guarnieri. 1993. Spontaneous myocardial calcium oscillations: are they linked to ventricular fibrillation? *J. Cardiovasc. Electrophysiol.* 4:473–489.

Lipp, P., and E. Niggli. 1996. A hierarchical concept of cellular and subcellular Ca(2+)-signalling. *Prog. Biophys. Mol. Biol.* 65:265–296.

López-López, J. R., P. S. Shacklock, C. W. Balke, and W. G. Wier. 1995. Local calcium transients triggered by single L-type calcium channel currents in cardiac cells. *Science.* 268:1042–1045.

Luo, C. H., and Y. Rudy. 1994. A dynamic model of the cardiac ventricular action potential. I. Simulations of ionic currents and concentration changes. *Circ. Res.* 74:1071–1096.

Lytton, J., M. Westlin, S. E. Burk, G. E. Shull, and D. H. Maclennan. 1992. Functional comparisons between isoforms of the sarcoplasmic or endoplasmic reticulum family of calcium pumps. *J. Biol. Chem.* 267: 14483–14489.

McCall, E., K. S. Ginsburg, R. A. Bassani, T. R. Shannon, M. Qi, A. M. Samarel, and D. M. Bers. 1998. Ca flux, contractility, and excitation-contraction coupling in hypertrophic rat ventricular myocytes. *Am. J. Physiol.* 274:H1348–H1360.

Merillat, J. C., E. G. Lakatta, O. Hano, and T. Guarnieri. 1990. Role of calcium and the calcium channel in the initiation and maintenance of ventricular fibrillation. *Circ. Res.* 67:1115–1123.

Nikolic, G., R. L. Bishop, and J. B. Singh. 1982. Sudden death recorded during Holter monitoring. *Circulation.* 66:218–225.

Pratt, C. M., M. J. Francis, J. C. Luck, C. R. Wyndham, R. R. Miller, and M. A. Quinones. 1983. Analysis of ambulatory electrocardiograms in 15 patients during spontaneous ventricular fibrillation with special reference to preceding arrhythmic events. *J. Am. Coll. Cardiol.* 2:789–797.

Rae, J., K. Cooper, P. Gates, and M. Watsky. 1991. Low access resistance perforated patch recordings using amphotericin B. *J. Neurosci. Methods.* 37:15–26.

Saitoh, H., J. C. Bailey, and B. Surawicz. 1989. Action potential duration alternans in dog Purkinje and ventricular muscle fibers. Further evidence in support of two different mechanisms. *Circulation.* 80:1421–1431.

Stern, M. D., M. C. Capogrossi, and E. G. Lakatta. 1988. Spontaneous calcium release from the sarcoplasmic reticulum in myocardial cells: mechanisms and consequences. *Cell Calcium.* 9:247–256.

Weiss, J. N., A. Garfinkel, H. S. Karaguezian, Z. Qu, and P. S. Chen. 1999. Chaos and the transition to ventricular fibrillation: a new approach to antiarrhythmic drug evaluation. *Circulation.* 99:2819–2826.

Wit, A. L., and M. J. Janse. 1993. The Ventricular Arrhythmias of Ischemia and Infarction: Electrophysiological Mechanisms. Futura Publishing Co., Mount Kisco, NY.

Yao, A., H. Matsui, K. W. Spitzer, J. H. Bridge, and W. H. Barry. 1997. Sarcoplasmic reticulum and Na+/Ca2+ exchanger function during early and late relaxation in ventricular myocytes. *Am. J. Physiol.* 273: H2765–H2773.

Zaza, A., M. Rocchetti, A. Brioschi, A. Cantadori, and A. Ferroni. 1998. Dynamic Ca2+-induced inward rectification of K+ current during the ventricular action potential. *Circ. Res.* 82:947–956.

Zeng, J., K. R. Laurita, D. S. Rosenbaum, and Y. Rudy. 1995. Two components of the delayed rectifier K+ current in ventricular myocytes of the guinea pig type. Theoretical formulation and their role in repolarization. *Circ. Res.* 77:140–152.

Zygmunt, A. C., and W. R. Gibbons. 1991. Calcium-activated chloride current in rabbit ventricular myocytes. *Circ. Res.* 68:424–437.